Int J Adv Manuf Technol (2013) 69:1203–1217
DOI 10.1007/s00170-013-5099-2

ORIGINAL ARTICLE

Decoupled chip thickness calculation model for cutting force prediction in five-axis ball-end milling

Tao Huang · Xiaoming Zhang · Han Ding

Received: 24 March 2013 / Accepted: 27 May 2013 / Published online: 14 June 2013

Abstract Cutting force prediction plays very critical roles for machining parameters selection in milling process. Chip thickness calculation supplies the basis for cutting force prediction. However, the chip thickness calculation in five-axis ball-end milling is difficult due to complex geometrical engagements between parts and cutters. In this paper, we present a method to calculate the chip thickness in five-axis ball-end milling. The contributions of lead and tilt angles in five-axis ball-end milling on the chip thickness are studied separately in detail. We *prove* that the actual chip thickness can be *decoupled* as the sum of the ones derived from the two individual cutting conditions, i.e., lead and tilt angles. In this model, the calculation of engagement boundaries of tool–workpiece engagement is easy; thus, time consumption is low. In order to verify the proposed chip thickness model, the chip volume predicted based on the proposed chip thickness calculation model is compared with the theoretical results. The comparison results show that the desired accuracy is obtained with the proposed chip thickness calculation model. The validation cutting tests, which are in a constant material removal rate and with only ball part engaged in cutting, are carried out. The optimized lead and tilt angles are analyzed with regard to cutting forces. The geometrical as well as the kinematics meaning of the proposed method is obvious comparing with the existing models.

Keywords Ball-end mill · Chip thickness · Tool inclination · Five-axis · Cutting force

T. Huang · X. Zhang (✉) · H. Ding
School of Mechanical Science and Engineering,
State Key Laboratory of Digital Manufacturing Equipment and Technology, Huazhong University of Science and Technology, Wuhan 430074, People's Republic of China
e-mail: cheungxm@hust.edu.cn

1 Introduction

Five-axis ball-end milling is used extensively in the manufacturing of three-dimensional (3D) free-form surfaces such as turbine engine components, dies, and molds. In most of these cases, the manufacturing tolerances are very tight due to the required high quality and dimensional integrity. In practice, to improve part quality and avoid undesirable results such as tool breakage or excessive deflection based on the resultant cutting forces in five-axis ball-end milling, the selection of process parameters is conservative, which comes at cost of lowering the productivity. Much effort has been devoted to the optimization of milling process based on cutting forces [1–7]. Hence, analysis of the cutting force in machining of free-form surface is critical for process planning in order to optimize the production rates and reduce the cost. Cutting force models for ball-end milling are based on the chip thickness, which is the thickness of the material removed instantaneously by the cutting edge in the normal direction.

Chip thickness calculation has been receiving great attention over the past several decades. The chip thickness calculation models can be divided into three types. *One is the solid modeling method*. Takata [8] used a solid modeling approach for 2.5-axis machining and feedrate scheduling as did by Spence and Altintas [9]. El Mounayri et al. [10] used a solid modeling system to compute the volume removed for a given three-axis tool path followed by a ray casting technique to compute the instantaneous chip thickness. Imani et al. [11] developed a simulation system for three-axis ball-end milling of sculptured surfaces using the ACIS solid modeling kernel. The authors used a NURBS curve to model the cutting edge of the tool. However, extracting the instantaneous chip thickness from the model was computationally inefficient, and therefore, the authors

relied on the simple geometry of a ball nose-end mill and restricted the simulations to inclined cuts.

The second type of chip thickness calculation is the discretization method, which employs discretization of the workpiece and the tool. Kim et al. [12] discussed the application of a Z-map to the prediction of three-axis ball-end milling forces, but relied heavily on the simple geometry of the sphere and linear movements. Fussell et al. [13] integrated an extended Z-buffer model representing the workpiece with a swept envelope of tool path to determine the contact area between cutter and workpiece for a given tool path in five-axis milling. In the simulation, with maintaining a desired level of accuracy, the five-axis tool movement is approximated by the three-axis to simplify calculations. Although Z-buffer algorithms have been implemented extensively for various kinds of mill cutters, different procedures for calculating the chip geometry are necessary for each method. To overcome the universality concerns of modeling techniques, an adaptive depth buffer method for mechanistic modeling of three-axis machining was presented by Roth et al. [14] and later generalized to five-axis machining using an adaptive and local depth buffer [15]. Antoniadis et al. [16] simulated precisely the tool kinematics and considered the effect of the cutting geometry on the resulting roughness by using the so-called MSN-Milling Software Needle program for ball-end milling. Guo et al. [17] presented a method to calculate the chip thickness in five-axis ball-end milling according to the real kinematic trajectory of cutting edges under continuous change of cutter axis orientation along the given tool path. Lazoglu et al. [18] presented a novel and generalized approach for prediction of cutting forces of complex free form surfaces machining. Engagement simulations between cutter and workpiece are performed precisely along the tool path by boundary representation method. Gonzalo et al. [19] used both mechanistic and numerical methods together to model a milling operation, which employed the FEM cutting model analyzed in the software AdvantEdge™.

However, all of these works involve a certain amount of computationally intensive Boolean operations and sophisticated curve/body intersection algorithms, and their accuracy is dependent to the grid size selected. *The third type of chip thickness calculation is the analytical method*, in which there is no need for a grid size selection; thus, there is no tradeoff between grid size and calculation time and the computation is high efficiency. Lamikiz et al. [20] proposed a model to estimate the cutting forces in inclined surfaces machining considering both up- and down-milling, which takes the piece slope effect into account. Fontaine et al. [21] determined the cutting forces by decomposing the working cutting edges into a series of axial elementary cutting edges based on a thermomechanical model of oblique cutting. The chip thicknesses are obtained by projecting the feed per tooth onto the normal vectors of the tool envelope at exact points. Yet, the experiments did not consider the situations with both lead and tilt angles.

Ozturk et al. [22] developed an analytical approach for determining the cutter/workpiece engagement region in the machining of 3D freeform monotonic surfaces with ball-end mill. Later, Ozturk et al. [23] studied the effects of lead and tilt angles on the engagement limits between the milling tool and the workpiece in five-axis ball-end milling process and predicted the cutting forces. Subrahmanyam et al. [24] investigated the cutting force for ball nose milling of inclined surface, which considered only the lead angle, and a method for the determination of the coefficients using the inclined plane milling data is proposed. Ferry and Altintas [25] presented a method to compute the chip thickness in five-axis flank milling by splitting the total chip thickness into horizontal and vertical feed components, and this model is adopted by Zhang [4] to predict cutting forces, tool deflections and optimize the feedrates. Tsai and Liao [26] analyzed the geometrical model in ball-end milling with inclined feed. The influences of changing different feed angles and helix angles on three-dimensional cutting force are simulated. In these works, essential rules of the engagement conditions of ball-end cutter with workpiece are not clear with both lead and tilt angles. Few literatures have evaluated the accuracy of the chip thickness calculation algorithm. Kurt and Bagci [7] declared it is inevitable that mechanistic force-based feedrate optimization approaches, for which the calculation time is improved, will be integrated into commercial CAM software packages. It indicates that the reduction of cutting force calculation time consumption is also important.

The contribution of this work is that we develop an analytical and efficient and geometrically intuitional model of chip thickness calculation in five-axis ball-end milling. First, in this model, the chip thickness is decoupled into two components determined by tilt and lead angles. The geometrical as well as the kinematics meaning of the proposed method is obvious comparing with the existing works. The differences between the proposed model and several existing analytical methods are analyzed in detail, and the proposed one shows better accuracy. The deviation of the model is assessed by a series of numerical calculation, Moreover, the exact engagement boundaries is determined at the same time when chip thicknesses are calculated. Then, cutting tests are conducted, in which a constant material removal rate is kept in order to validate the chip thickness model as well as to investigate the effects of lead and tilt angles on the cutting forces. The process of cutter tooth engaging in the workpiece is figured out and how it influences the cutting forces are discussed. The optimized lead and tilt angles are obtained with regard to cutting forces.

The rest of this paper is organized as follows. In Section 2, the representation of coordinate systems is given as the basis to the geometry analysis of five-axis milling operations. Section 3 presents the method of chip thickness calculation in a five-axis slot milling. The cutting process is divided into two individual motions, with only tilt angle and only lead angle, and the contributions of each one are studied in detail. In Section 4, boundaries of workpiece–cutter engagement region are determined in order to extend the proposed method from the five-axis slot milling operation to a general five-axis one. In order to verify the proposed chip thickness model, the chip volume predicted based on the proposed model is compared with the theoretical results in Section 5. In Section 6, validation tests are carried out, the effects of lead and tilt angles on the cutting forces are analyzed in detail. Conclusions are reached in Section 7.

2 Representation of coordinate systems

In order to determine instantaneous engagement regions, one has to present the ball-end cutter and workpiece coordinate systems. Ball-end cutter and workpiece are represented with different Cartesian coordinates. Actually, there are at least three coordinates needed to define the position and orientation of the cutter in the milling process. The first one is a fixed coordinate system, MCS, formed by the (X), (Y), and (Z) axes of the machine tool. The second one is the process coordinate system, FCN, consisting of feed (F), cross-feed (C), and surface normal (N) axes. Finally, TCS is the tool coordinate system, which is the rotated form of the FCN. In TCS, the tool axis is the (z) axis of this coordinate system where (x) and (y) axes are in the transversal directions of the cutting tool, while (y) and (z) axis are coplanar with (N) axes.

In five-axis ball-end milling, the tool tip contact with the workpiece should be avoided as the contact can result in extra-indentation and ploughing forces [27, 28] as well as tool tip marks on the resulting surfaces. To avoid tool tip contact as well as tool–workpiece collision, the tool inclination is adopted. The tool orientation is determined by lead and tilt angles, which are measured with respect to the surface normal axis (N). The lead angle is the rotation of the tool axis about the cross-feed axis (C), and the tilt angle is the rotation about the feed axis (F). In this paper, α and γ as shown in Fig. 1, are used to determine the tool orientation, which are equivalent to the traditional representations of lead and tilt angles, as stated in [29]. The coordinate translation matrix is represented:

$$\begin{bmatrix} F \\ C \\ N \end{bmatrix} = \begin{bmatrix} -\sin\gamma & -\cos\gamma\cos\alpha & \cos\gamma\sin\alpha \\ \cos\gamma & -\sin\gamma\cos\alpha & \sin\gamma\sin\alpha \\ 0 & \sin\alpha & \cos\alpha \end{bmatrix} \begin{bmatrix} x \\ y \\ z \end{bmatrix} \tag{1}$$

As discussed in the literature, positive lead angles are favorable to avoid tool tip contact [23]. In the representation with α and γ, it means that the angle γ should be better in the range $\left(-\frac{\pi}{2}, \frac{\pi}{2}\right)$. We only consider γ in the range $\left(-\frac{\pi}{2}, \frac{\pi}{2}\right)$ in the remainder of this paper.

For a ball-end cutter, local radius is zero at tool tip and increases along the tool axis in the ball part and has a constant value in the cylindrical part. In our discussions, the cutting condition and chip thickness of the cylindrical part are not mentioned. However, the approach proposed here can be utilized to solve it similarly.

3 Chip thickness calculation with tool inclination

In the case with tool–surface inclination, the intersection curve between the hemisphere and workpiece surface is a circle, which is shown in Fig. 2. The center is stated as O'. Line $O'A'$ is the projection of tool axis on the workpiece surface. In Fig. 2a, the direction of feed per teeth f is along the F axis. The blue region means the cutting contact area, which has positive effect on chip thickness, while the yellow region means the tool moves away from workpiece and has negative effect on chip thickness. In order to calculate the chip thickness, the cutting process is divided into two resolved motions: one is the milling with only tilt angle (Fig. 2b), and the other is with only lead angle (Fig. 2c).

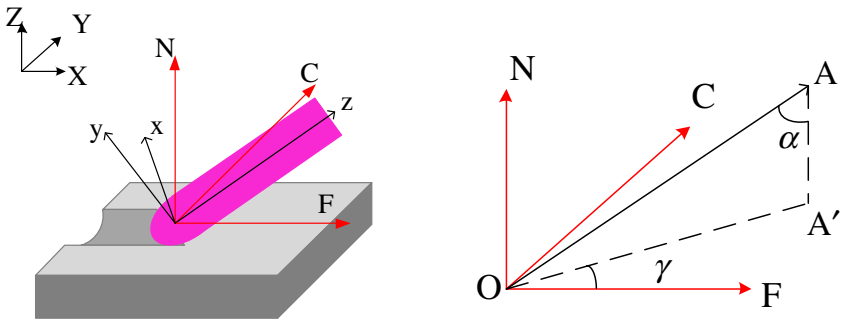

Fig. 1 Representation of tool inclination

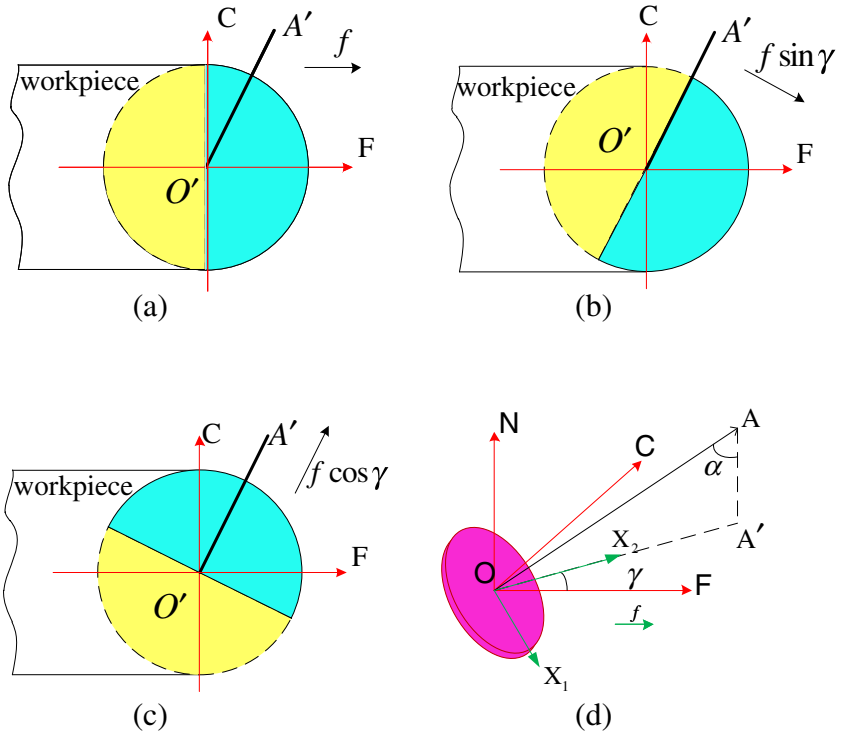

Fig. 2 Decomposed motion and the engagement regions

The disc movement after the decomposition is shown in Fig. 2d. The feed vector f can then be decomposed into two components, f_t along unit vector $\{OX_1\}$ and f_l along unit vector $\{OX_2\}$ which can be expressed by:

$$\begin{aligned}\{OX_1\} &= \frac{\{z\}\times\{N\}}{\|\{z\}\times\{N\}\|}, f_t = \{OX_1\} f\sin\gamma \\ \{OX_2\} &= \frac{\{N\}\times\{OX_1\}}{\|\{N\}\times\{OX_1\}\|}, f_l = \{OX_2\} f\cos\gamma\end{aligned} \tag{2}$$

where f_t denotes the feed with only tilt angle and f_l the feed with only lead angle.

For those engaged cutting edge element, the chip thickness model determines the instantaneous undeformed chip thickness distribution along the cutting edges. The uncut chip thickness at a certain location along the cutting edge on ball part can be approximated as $h_j(\varphi,\theta)=f\sin\varphi_j(\theta)\sin\theta$ if feed direction is perpendicular to the tool axis, without lead and tilt angles, where f is the feed per tooth and $\varphi_j(\theta)$ is the immersion angle for the flute (j) at disc position angle θ. For a specific disc, the uncut chip thickness is known if we get the radial uncut chip thickness $h_j(\varphi,\theta)/\sin\theta$, which is perpendicular to the cutter axis. Hence, chip thickness of a disc in the following words refers to the radial uncut chip thickness equal to $h_j(\varphi,\theta)/\sin\theta$.

As discussed above, the uncut chip thickness of a disc can be either positive or negative. In Fig. 2a–c, we can see that the blue region dictates the area on ball part where the discs have positive uncut chip thickness, yet the yellow region the area where the discs have negative one. Then, the uncut chip thickness of a disc can expressed as the sum of uncut chip thickness distributed from two decomposed motions respectively:

$$h = h_t + h_l \tag{3}$$

where h_t is the chip thickness distributed from the motion with only tilt angle, and h_l is the one distributed from the motion with only lead angle. The calculation of h_t and h_l are discussed in detail later. The disc is engaged in cutting when h is greater than zero, while it is not at the condition h is less than or equal to zero. In five-axis ball-end milling, lead and tilt angles result in the complicated uncut chip thickness. In

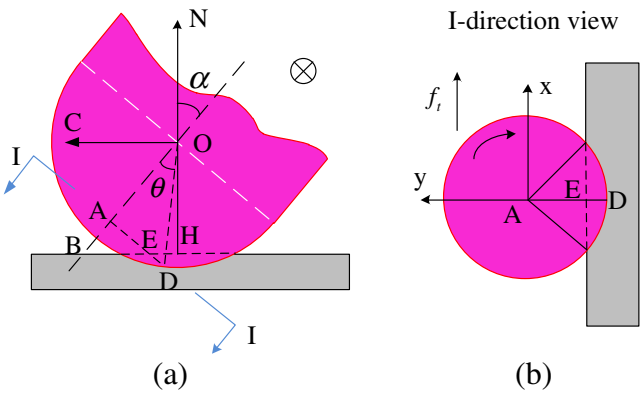

Fig. 3 Cutting condition of discs in milling with only tilt angle

the following discussions, we will use a straightforward way to study the effects of tilt and lead angles on chip thickness, with a geometrical intuitional meaning.

3.1 Tilt angle effect on chip thickness

Tilt angle effect in milling process is shown in Fig. 3, where lead angle is eliminated and $\gamma=\pi/2$. The position angle of the disc that participates in cut satisfies $\theta_s \le \theta \le \theta_e$. The lower and upper limits can be calculated by:

$$\begin{cases} \theta_s = \max\left\{\alpha - \arccos\dfrac{|OH|}{R}, 0\right\} \\ \theta_e = \alpha + \arccos\dfrac{|OH|}{R} \end{cases} \tag{4}$$

where R is the radius of cylindrical part of the ball-end cutter. The cutting radius of the disc at position angle θ is described as $R_\theta=|AD|=R\sin\theta$. The start and exit immersion angles of the disc can be stated as:

$$\begin{cases} \Phi_{st} = \arccos\left(\min\left\{\dfrac{y_E}{R_\theta}, 1\right\}\right) \\ \Phi_{ex} = 2\pi - \Phi_{st} \end{cases} \tag{5}$$

where y_E is the y coordinate of pedal point E (as shown in Fig. 3b):

$$\begin{aligned} |AE| &= |OH|\frac{|AB|}{|HB|} = |OH|\frac{|OB|-|OA|}{|OH\tan\alpha|} \\ &= \frac{|OH\sec\alpha|-|R\cos\theta|}{\tan\alpha} \end{aligned} \tag{6}$$

As shown in Fig. 3b, the chip thickness is positive from Φ_{st} to π (point D) and negative from π (point D) to Φ_{ex}. It can be described as follows:

$$h_t = f_t\sin\varphi_j(\theta) + R_\theta - \sqrt{R_\theta{}^2 - \left(f_t\cos\varphi_j(\theta)\right)^2} \tag{7}$$

where $\varphi_j(\theta)$ is in the range $\Phi_{st} \le \varphi_j(\theta) \le \Phi_{ex}$.

3.2 Lead angle effect on chip thickness

The angle $\gamma=0$ when only lead angle arise. The material removed by a tooth of a disc at position angle θ is not based on path formed by the previous tooth of the same disc, but another disc at a position angle θ' (Fig. 4), which has greater radius. The relation between θ' and θ can be expressed by equations as follows:

$$\begin{aligned} \pm f_\theta &= R\sin\theta + f_l\cos\alpha - R\sin\theta' \\ R\cos\theta &= R\cos\theta' + f_l\sin\alpha \end{aligned} \tag{8}$$

where $\pm f_\theta$ is the radial feed per tooth at position angle θ. The plus sign is applied in the positive blue region, while the minus sign in negative yellow region. Then, f_θ and θ satisfy the following equation derived from Eq. (8):

$$(R\sin\theta + f_l\cos\alpha \mp f_\theta)^2 + (R\cos\theta - f_l\sin\alpha)^2 = R^2 \tag{9}$$

In milling with only lead angle, the radial feed per tooth of each disc varies at different position angle θ. The four

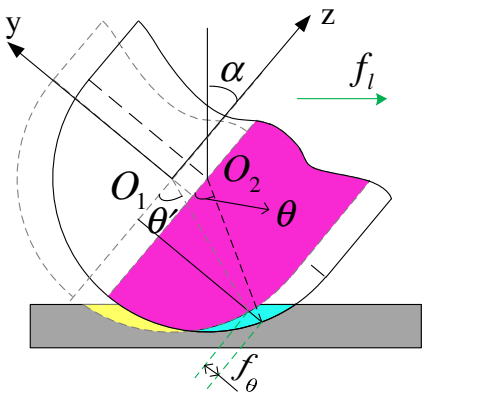

Fig. 4 Radial feed per tooth relates to the previous tooth in milling with only lead angle

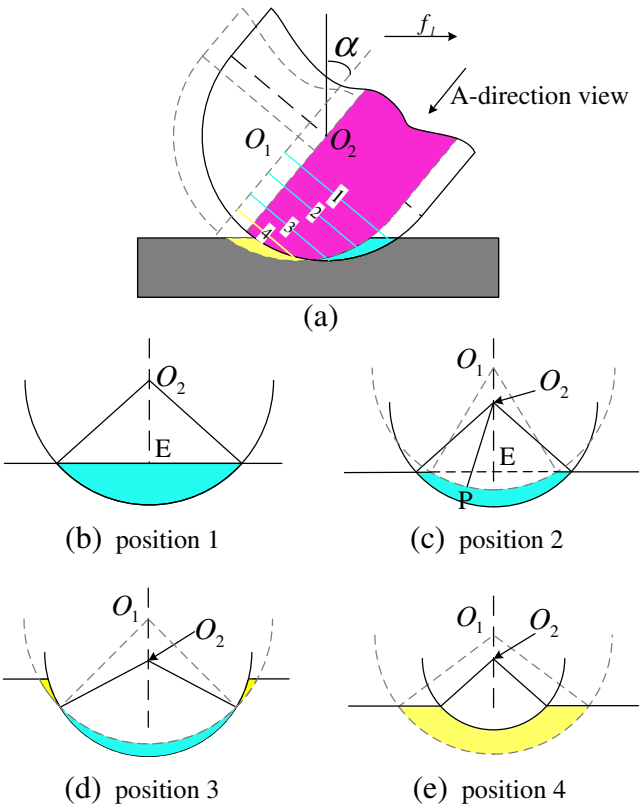

Fig. 5 Cutting condition of discs in lead angle milling

positions with different cutting conditions are shown in Fig. 5. The cutting characteristics of the four typical discs are described respectively as follows.

In milling with only lead angle, the range of position angle θ of a disc, which participates in cut is as same as the one in milling with only tilt angle (Eq. (4)). The start immersion angle Φ_{st} and exit immersion angle Φ_{ex} of a disc can also be calculated using Eq. (5).

3.2.1 Position 1

As shows in Fig. 5b, the material removed by the tooth has nothing to do with the previous tooth. Position angle θ satisfies:

$$\arccos\frac{R\cos\theta_e + f_1\sin\alpha}{R} \le \theta < \theta_e \tag{10}$$

where θ_e is calculated using Eq. (4). The start Φ_{st} and exit angle Φ_{ex} of disc 1 are calculated using Eq. (5).

When the immersion angle $\varphi_j(\theta)$ satisfies the condition $\Phi_{st} \le \varphi_j(\theta) \le \Phi_{ex}$, the chip thickness can be expressed as:

$$h_1 = R\sin\theta + \frac{|O_2E|}{\cos\varphi_j(\theta)} \tag{11}$$

$|O_2E|$ using Eq. (6) by replacing point A with point O_2. The value of h_1 is always positive.

3.2.2 Position 2

In position 2 (as shown in Fig. 5c), position angle θ satisfies:

$$\arccos\frac{|OH|\cos\alpha}{R} \le \theta < \arccos\frac{R\cos\theta_e + f\sin\alpha}{R} \tag{12}$$

There are two different cutting conditions. The first condition happens when the tooth begins to start in or exit out of immersion. That means when the immersion angle $\varphi_j(\theta)$ satisfies:

$$\Phi_{st} < \varphi_j(\theta) \le \pi - \arctan\frac{\sqrt{R_{\theta'}{}^2 - \left|O_1E\right|^2}}{\left|O_1E\right| - f_1\cos\alpha}$$

$$\text{or } \pi + \arctan\frac{\sqrt{R_{\theta'}{}^2 - \left|O_1E\right|^2}}{\left|O_1E\right| - f_1\cos\alpha} \le \varphi_j(\theta) < \Phi_{ex}$$

For the first condition, the cutting condition is the same as that in the position 1, so the chip thickness can be calculated using Eq. (11). The value of h_1 is always positive. The second condition happens when the engagement relates to the previous cut, and $\varphi_j(\theta)$ satisfies:

$$\pi - \arctan\frac{\sqrt{R_{\theta'}{}^2 - \left|O_1E\right|^2}}{\left|O_1E\right| - f_1\cos\alpha} < \varphi_j(\theta)$$

$$< \pi + \arctan\frac{\sqrt{R_{\theta'}{}^2 - \left|O_1E\right|^2}}{\left|O_1E\right| - f_1\cos\alpha}$$

then the chip thickness has:

$$h_1 = R\sin\theta - |O_2P| \tag{13}$$

where $|O_2P|$ is obtained by:

$$|O_2P|^2 + (f_1\cos\alpha)^2 - 2|O_2P|f_1\cos\alpha\cos\varphi = \left(R\sin\theta'\right)^2 \tag{14}$$

The value of h_1 is always positive.

3.2.3 Position 3

As shows in Fig. 5d, the chip thickness is negative in a period that the tooth starts in or exits out of immersion, while positive in the rest period. Position angle θ satisfies:

$$\alpha - \arcsin\frac{f_1}{2R} \le \theta < \arccos\frac{|OH|\cos\alpha}{R} \tag{15}$$

where α is the lead angle. The chip thickness can be calculated using Eq. (13). The value of h_1 can be either positive or negative.

3.2.4 Position 4

As shown in Fig. 5e, the chip thickness relates to the previous cut and has negative value. Position angle θ satisfies:

$$\theta_s < \theta < \alpha - \arcsin\frac{f_1}{2R} \tag{16}$$

The chip thickness can be calculated using Eq. (13). The value of h_1 is always negative.

Four positions indicate the different cutting conditions of element discs engaged in cutting. To make a comparison with two frequently used methods of uncut chip thickness calculation in [23] and [25], the differences of this work from the related works are declared in detail. Ozturk and Budak

[23] determined the uncut chip thickness ct at a point q on the cutting edge by the product of the feed vector $\vec{t}$ and the unit outward surface normal vector $\vec{u}$ of the tool at the cutting point (Fig. 5 in [23]). However, considering a point q on intersecting curve of cutter surface with the surface of workpiece, take the case of position 1 as an example, the start point of vector $\vec{ct}$ (see Fig. 5 in [23]), which is on the cutter surface of previous cutting position, is not engaged in cutting at that time actually. Thus, uncut chip thickness given by ct is greater than the actual one. The deviation induced by this approximation increases with greater inclination angle α according to the analysis above. On the other hand, Ferry and Altintas [25] presented a method to compute the chip thickness in five-axis flank milling by splitting the total chip thickness into horizontal and vertical feed components. The cutting conditions of an element throughout the cutting process are treated as the same, i.e., the start in and exit out of immersion cutting conditions were not discussed separately; thus, deviation grows. For instance, at positions 1 and 2, the uncut chip thicknesses are calculated with specific expressions when cutter flutes start in or exit out of immersion in this work. With the method in reference [25], some redundant material is added. The ignorance of the effect of start or exit is not significant in [25] because of the large axial depth of cut in flank milling. However, in ball-end milling, the deviation is relatively more considerable with much smaller chip volume. The conclusion that the deviation increases with greater radial cutting depth and greater feed rate per tooth is reached from the analysis in this work. Furthermore, the horizontal and vertical feed components include feed velocity components in the normal direction of the machined surface, which lead to a different engagement boundaries from current cutting position to the previous one, even in a flat surface machining. Thus, the further analysis of chip thicknesses is more complex. As a comparison, the decomposed feed components in this work are tangential to the machined surface.

4 Boundaries of engagement region

From the discussion in the previous sections, it is clear that the total chip thickness has the value of zero on the boundaries of engagement region. However, relative boundaries, out of which the tooth will absolutely be not engaged in cutting and within which the tooth will be possibly engaged in cutting, should be obtained before the calculation. As shown in Fig. 6, the relative boundaries consist of curve C1 (in blue) and C2 (in red), where C1 shows the intersection curve between ball-end cutter and the previous machined tool path surface, while C2 shows the intersection curve between the cutter and the uncut workpiece surface after previous machining. Considering a disc element as a circle, intersection points of the circle with a plane or a cylindrical surface are obtained from analytical solutions of quadratic equations.

Each point P (Fig. 6) on the relative boundaries belongs to an exact disc with position angle θ, which can be calculated as follows:

$$\theta = \arccos \frac{\{PO\}\{z\}}{\|\{PO\}\{z\}\|} \tag{17}$$

where the vector $\{PO\}$ is from point P to the center point O of the semisphere of the cutter, and $\{z\}$ is the vector of the tool axis. The immersion angle of a tooth at the boundary point P can be calculated:

$$\begin{cases} \Phi(P) = \arccos \dfrac{\{z\} \times \{OP\} \times \{z\}\{y\}}{\|\{z\} \times \{OP\} \times \{z\}\{y\}\|}, x_P > 0; \Phi(P) = \pi, x_P = 0; \Phi(P) = 2\pi - \arccos \dfrac{\{z\} \times \{OP\} \times \{z\}\{y\}}{\|\{z\} \times \{OP\} \times \{z\}\{y\}\|}, x_P < 0 \end{cases} \tag{18}$$

where $\{y\}$ is the y axis of tool coordinate system TCS. x_P is the x coordinate of point P in tool coordinate system TCS.

Hereto, the relative boundaries are modeled. In order to get the exact boundaries of engagement region, the calculation of chip thickness is adopted. The points at which the chip thickness is zero and within the relative boundaries are extracted as the exact engagement boundary points.

By this means, the calculation of engagement boundaries is much easier. As a comparison, Ozturk and Lazoglu [22] developed an analytical approach for determining the tool–workpiece engagement region in the machining of 3D freeform monotonic surfaces with ball-end mill. The boundaries of engagement surfaces, depending on whether process is in constant z value or downward motion or upward motion, are presented for the three cases separately. Three boundaries are discussed in detail for each case. While in this work, only two relative boundaries, which are not the exact ones and easier in calculation, are determined. On the other hand, both lead and tilt angles are considered in this work, while tilt angle is neglected in [22]. Ozturk and Budak [23] presented a unified formula in chip thickness calculation and developed a series of inequalities for determination of engagement boundaries correspondingly. However, the method given in [23] cannot be employed directly to handle the thickness calculation in our work because of utilization of various chip thickness calculation formulas.

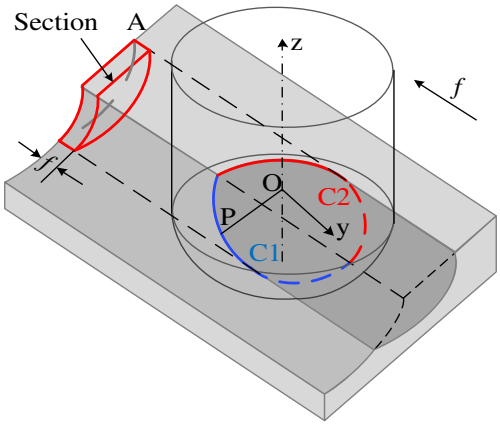

Fig. 6 Chip volume and intersection curve between cutter and workpiece

5 Verification and example applications

In order to verify the proposed chip thickness model, the chip volume predicted using this model is compared with the theoretical results. Because the volume of residual material between teeth is quite smaller than static chip volume, an ideally cut-off volume per tooth is illustrated in Fig. 6 as an approximate measurement of chip volume. It is equivalent to the volume that is extruded by length of the feed per tooth from its orthogonal section A as shown in Fig. 6. The theoretical volume, denoted as V_f is given as:

$$V_f = fS_A \tag{19}$$

where S_A is the exact area of section A. The predicted chip volume, denoted as V_p based on the proposed method can be calculated:

$$V_p = \sum_{h_r(\varphi,\theta)>0} h_r(\varphi,\theta)\Delta S \tag{20}$$

where

$$h_r(\varphi,\theta) = h(\varphi,\theta)\sin\theta = [h_l(\varphi,\theta) + h_t(\varphi,\theta)]\sin\theta$$
$$\Delta S = R_\theta \Delta\varphi R\Delta\theta = R^2 \sin\theta \Delta\varphi\Delta\theta$$

From the discussions in Section 3.1, the cutting of a disc in milling with only tilt angle is based on the tooth path formed by the previous tooth of the same disc. In reality, when there are both lead and tilt angles in the cutting operation, the previous tooth path is not formed by the tooth of the same disc, but another disc that has greater radius. Hence, the volume given by the proposed method (Eq. (20)) will be theoretically greater than the theoretical results.

5.1 Case 1

The slot milling is utilized and the cutting tool is a 10-mm diameter ball-end cutter with helix angle 30° and left spiral. The depth of cut and the cutting speed are constant at a_p=1 mm and

Table 1 Volumes calculated on different discrete intervals and error ranges

V_p (e−10m^3)	α=10°	α=20°	α=30°	α=40°	α=50°
$\Delta\varphi$=3°, $\Delta\theta$=3°					
γ=0°	4.179	4.064	4.255	4.187	4.194
γ=10°	4.178	4.066	4.256	4.189	4.198
γ=20°	4.183	4.076	4.259	4.197	4.200
γ=30°	4.187	4.095	4.264	4.206	4.201
γ=40°	4.192	4.116	4.271	4.218	4.202
γ=50°	4.192	4.135	4.271	4.224	4.202
γ=60°	4.188	4.149	4.263	4.227	4.199
γ=70°	4.184	4.161	4.248	4.225	4.194
γ=80°	4.185	4.171	4.226	4.224	4.185
γ=90°	4.187	4.177	4.209	4.224	4.180
Error range	−0.59–4.48 %				
$\Delta\varphi$=1°, $\Delta\theta$=3°					
γ=0°	4.171	4.063	4.229	4.216	4.226
γ=10°	4.170	4.067	4.232	4.216	4.227
γ=20°	4.174	4.076	4.236	4.220	4.231
γ=30°	4.178	4.091	4.240	4.225	4.237
γ=40°	4.182	4.107	4.243	4.232	4.241
γ=50°	4.182	4.124	4.242	4.235	4.244
γ=60°	4.178	4.137	4.238	4.234	4.243
γ=70°	4.174	4.149	4.227	4.229	4.239
γ=80°	4.176	4.159	4.209	4.222	4.234
γ=90°	4.180	4.166	4.196	4.217	4.230
Error range	−0.61–3.82 %				
$\Delta\varphi$=1°, $\Delta\theta$=1°					
γ=0°	4.144	4.158	4.165	4.173	4.175
γ=10°	4.146	4.161	4.167	4.176	4.176
γ=20°	4.151	4.168	4.173	4.207	4.183
γ=30°	4.157	4.178	4.181	4.215	4.194
γ=40°	4.163	4.186	4.189	4.222	4.222
γ=50°	4.167	4.192	4.195	4.227	4.227
γ=60°	4.168	4.193	4.197	4.229	4.229
γ=70°	4.167	4.189	4.194	4.227	4.228
γ=80°	4.167	4.185	4.188	4.222	4.226
γ=90°	4.168	4.183	4.184	4.218	4.224
Error range	1.37–3.54 %				
$\Delta\varphi$=1°, $\Delta\theta$=0.5°					
γ=0°	4.162	4.155	4.162	4.171	4.181
γ =10°	4.163	4.157	4.164	4.174	4.182
γ=20°	4.168	4.165	4.170	4.193	4.188
γ=30°	4.173	4.175	4.179	4.202	4.196
γ=40°	4.177	4.192	4.188	4.211	4.213
γ=50°	4.179	4.195	4.196	4.218	4.218
γ=60°	4.177	4.194	4.203	4.222	4.221
γ=70°	4.173	4.188	4.198	4.222	4.222
γ=80°	4.170	4.180	4.189	4.219	4.220
γ=90°	4.169	4.176	4.183	4.213	4.217
Error range	1.64–3.28 %				

Table 2 Volumes calculated with different process parameters

Volume and error	V_f	V_p	Error (%)
a_p=2 mm, f=0.2 mm	22.36	23.12	3.40
a_p=2 mm, f=0.1 mm	11.18	11.36	1.61
a_p=1.5 mm, f=0.2 mm	14.78	15.30	3.52
a_p=1.5 mm, f=0.1 mm	7.39	7.55	2.17

f=0.1 mm per tooth, respectively. Then, the volume calculated using Eq. (19) is given by V_f=4.088e−10 m^3. The volumes predicted by Eq. (20) with different discrete intervals are listed in Table 1. The prediction error can be approximated given by:

$$\text{err} = \left(V_p - V_f\right) \Big/ V_f \times 100\% \tag{21}$$

It is obvious that the error range becomes narrow with the smaller of discrete interval. It is shown in Table 1 that the volume calculated has a deviation about 1.64–3.28 % greater than the theoretical value, and this coincides with the previous discussion. The model error will be <5 % with discrete interval $\Delta\varphi$=3° and $\Delta\theta$=3°.

5.2 Case 2

Some other cases with different process parameters are tested with the proposed method, and the results are listed in Table 2. The discrete intervals are chosen to be $\Delta\varphi$=1°, $\Delta\theta$=1°, and inclination angles are set to be α=30°, γ=30°. It shows that the volume errors are at the same level with those presented in Table 1.

5.3 Case 3

In the remaining of this section, the results for the chip thickness calculation of several examples for *following cut operation* are addressed. Step over is set to be half of cutter diameter and cross-feed direction is positive. The cutting tool is a 10-mm diameter ball-end mill with helix angle 30°and left spiral. The depth of cut and the cutting speed were constant at 1 and 0.1 mm per tooth, respectively. Process parameters and tool–workpiece inclinations involved are listed in Table 3.

Table 3 Process parameters for following cut

Parameters and unit	value
Cutter diameter (mm)	10
Feed per tooth (mm)	0.1
Cross feed (mm)	5
Cutting depth (mm)	1
Inclination angle α (deg)	0–50
Inclination angle γ (deg)	−90–90

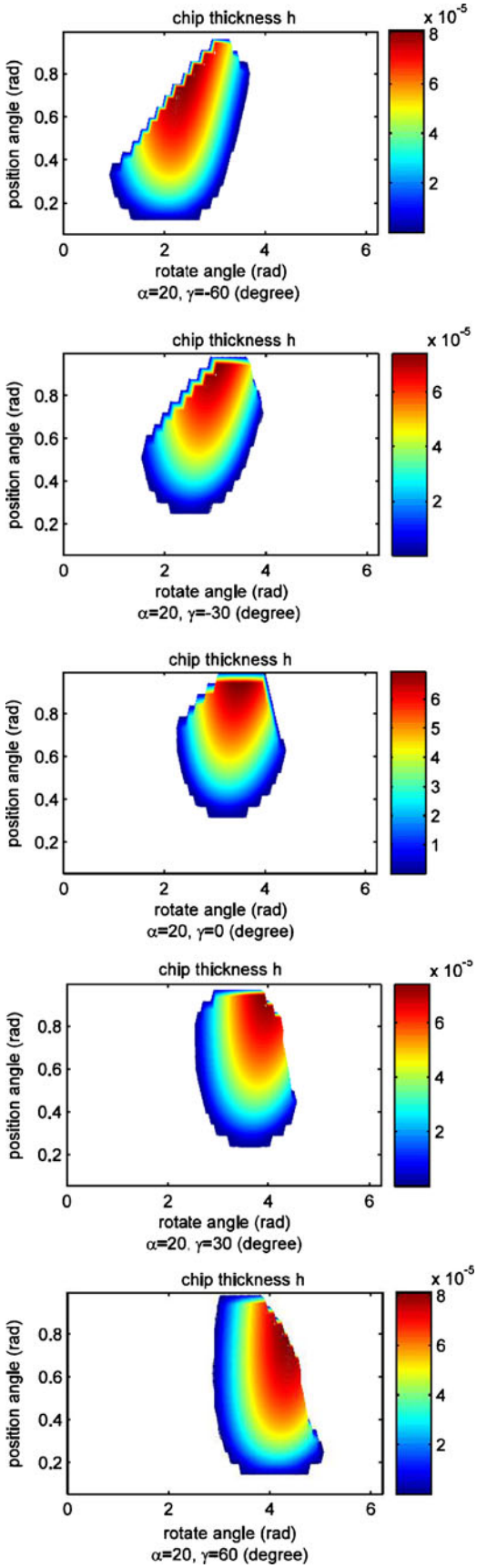

Fig. 7 Chip thickness of discs in a rotation period

Table 4 Volumes of the following cut operation and errors

	α=20°					α=40°				
γ	−60°	−30°	0°	30°	60°	−60°	−30°	0°	30°	60°
Volume e−10 m^3	4.02	3.94	3.88	3.92	3.97	4.02	4.02	4.05	4.00	4.00
Error (%)	2.55	0.51	−1.02	0	1.27	2.55	2.55	3.32	2.04	2.04

The cutting conditions of discs in a rotation period are shown in Fig. 7. X and Y axes label the rotation angle of the tool and the position angle of discs, respectively. The positive chip thicknesses are given with color bar. The discrete intervals are chosen to be $\Delta\varphi=\Delta\theta=3°$.

In the process with parameters in Table 3, the theoretical volume given by Eq. (19) results in V_f=3.92e−10 m^3. The volumes calculated using the proposed method, as well as the errors, are shown in Table 4. We can see that the chip thickness model for the following cut operation has the same error level comparing with the slot milling.

From Fig. 7, we conclude that the chip thicknesses at most disc elements are reduced to zero as the tool rotates, while the angle γ is negative, yet most of them are increased from zero while the angle γ is positive. Another difference between the cases with negative or positive angle γ is the contact duration of a tooth with workpiece, especially with greater angle α in the last five pictures of Fig. 7. It can be seen that the contact duration in the case with negative angle γ is longer than that with positive angle γ. Thus, the chip volume removed by a tooth is relatively dispersed and the maximum cutting forces is reduced with a negative angle γ. This is confirmed with the cutting experiments in Section 6.

6 Results of cutting experiments and simulations

The experiments for validation were performed on Mikron UCP800 Vertical Machining Center. In order to verify the model, five-axis ball-end milling tests on Al-7075 aluminum alloy were performed. The cutter was two fluted carbide ball-end mill cutter with 12 mm diameter, 37 mm projection length and 30° nominal helix angle (R216.42-12030-AK22A, Sandvik). A Kistler table type dynamometer (type 9257A) was used to measure cutting forces.

Cutting forces are calculated by cutting edges discretization. The cutting edge is discretized as a sequence of linear segments. For each segment, a set of simple expressions is used for the calculation of the cutting forces of the kind shown in Eq. (22). Expressions presented by Lee and Altintas [30], which are wildly used for cutting forces calculation and milling process optimization such as in [1, 5, 18, 19, 31–33], are

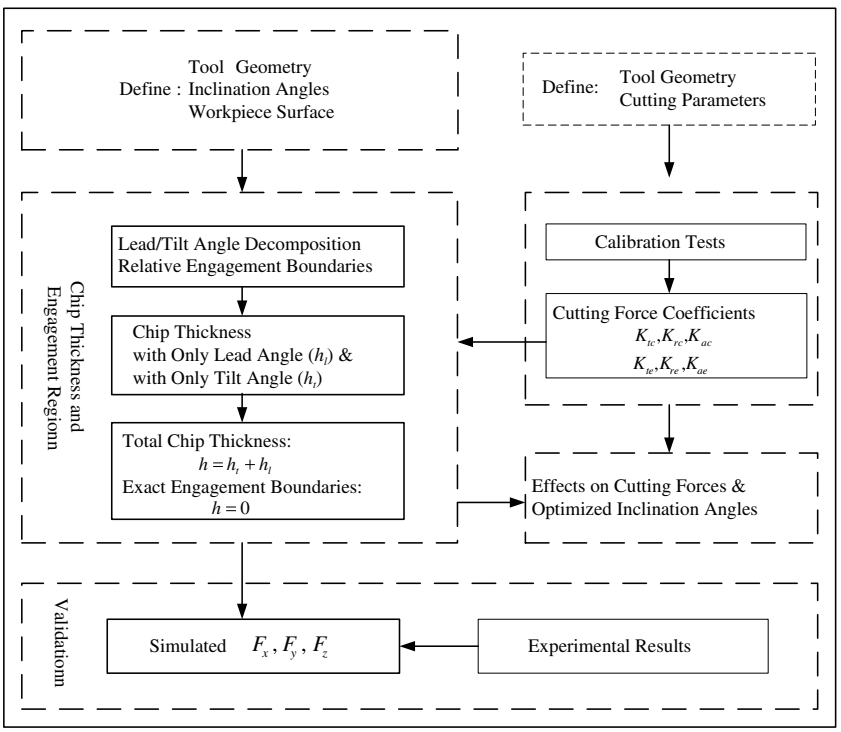

Fig. 8 The chart of the model simulation and validation

Table 5 Parameters of characterization tests

Test code	Depth of cut (mm)	Feed per tooth (mm/z)	Test code	Depth of cut (mm)	Feed per tooth (mm/z)
Al7075-1.1	1	0.03	Al7075-2.4	4	0.07
Al7075-1.2	2	0.03	Al7075-2.5	5	0.07
Al7075-1.3	3	0.03	Al7075-2.6	6	0.07
Al7075-1.4	4	0.03	Al7075-3.1	1	0.1
Al7075-1.5	5	0.03	Al7075-3.2	2	0.1
Al7075-1.6	6	0.03	Al7075-3.3	3	0.1
Al7075-2.1	1	0.07	Al7075-3.4	4	0.1
Al7075-2.2	2	0.07	Al7075-3.5	5	0.1
Al7075-2.3	3	0.07	Al7075-3.6	6	0.1

Table 6 Lead and tile angles of cutting tests

Lead (deg)	Tilt (deg)	α (rad)	γ (rad)	Lead (deg)	Tilt (deg)	α (rad)	γ (rad)
10	−40	0.7088	1.3637	30	−40	0.7946	0.9681
	−30	0.5431	1.2744		−30	0.6847	0.7854
	−20	0.3843	1.1197		−20	0.5989	0.5625
	−10	0.2444	0.7854		−10	0.5431	0.2964
	0	0.1745	0		0	0.5236	0
	10	0.2444	−0.7854		10	0.5431	−0.2964
	20	0.3843	−1.1197		20	0.5989	−0.5625
	30	0.5431	−1.2744		30	0.6847	−0.7854
	40	0.7088	−1.3637		40	0.7946	−0.9681
20	−40	0.7408	1.1615	40	−30	0.7946	0.6027
	−30	0.5989	1.0083		−20	0.7408	0.4093
	−20	0.4754	0.7854		−10	0.7088	0.2071
	−10	0.3843	0.4511		0	0.6981	0
	0	0.3491	0		10	0.7088	−0.2071
	10	0.3843	−0.4511		20	0.7408	−0.4093
	20	0.4754	−0.7854		30	0.7946	−0.6027
	30	0.5989	−1.0083				
	40	0.7408	−1.1615				

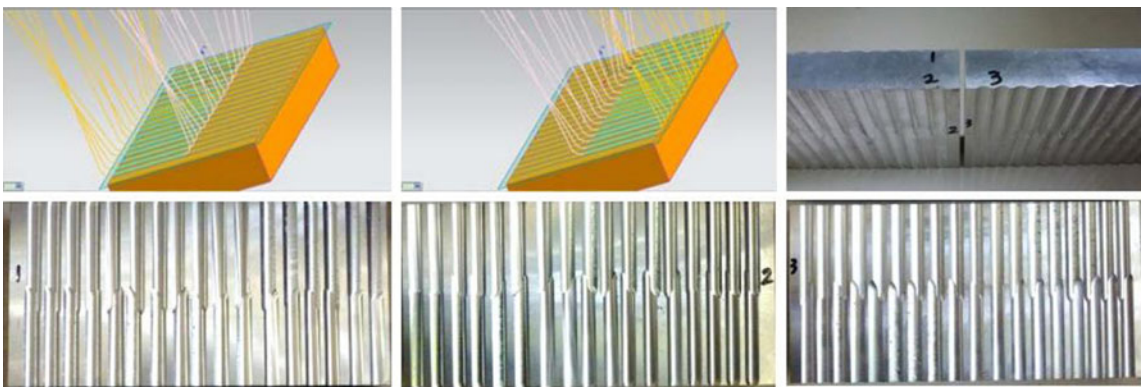

Fig. 9 Generated tool paths and the machined workpieces

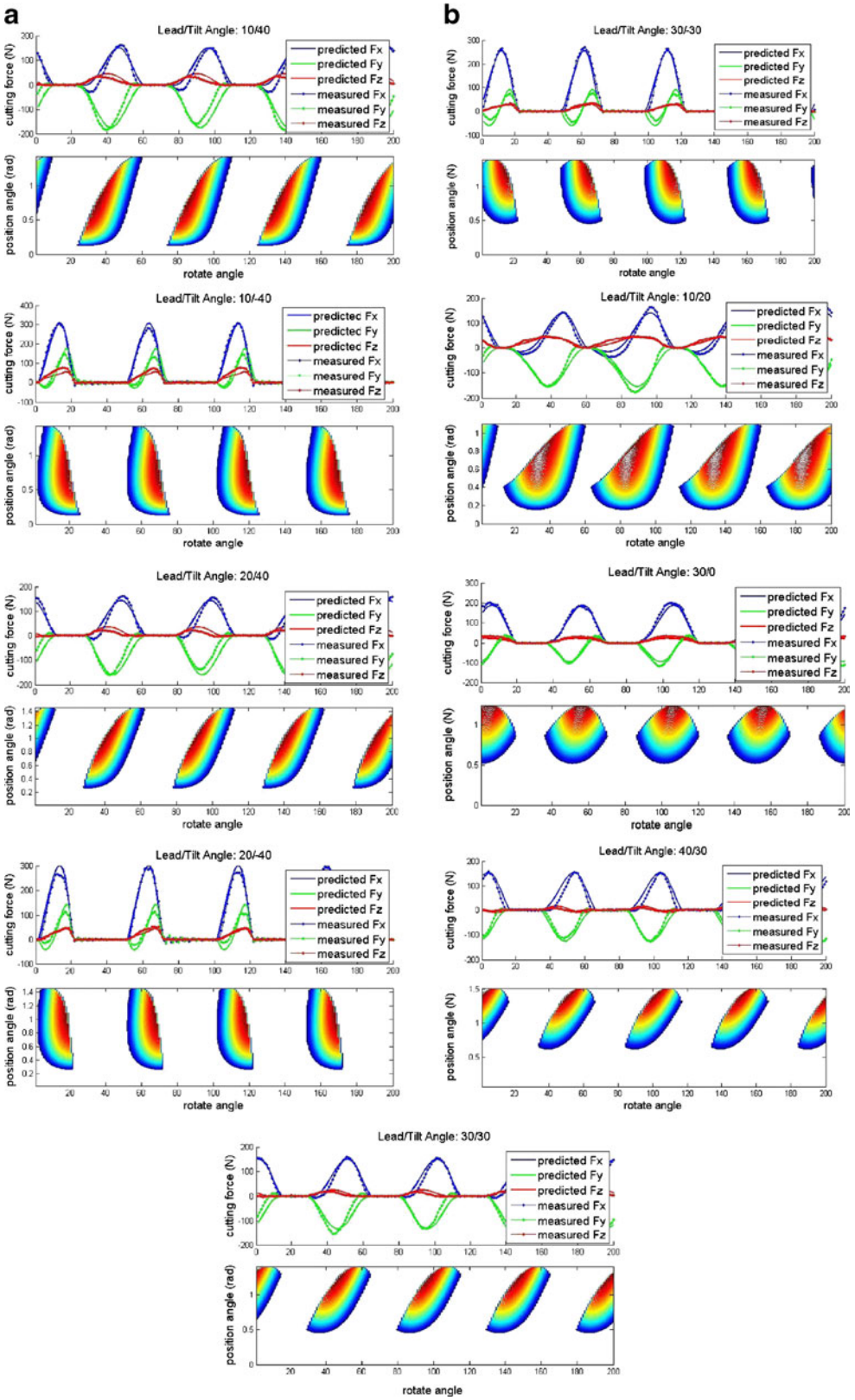

Fig. 10 Comparison of measured and predicted cutting forces and contact areas

adopted for the calculation of cutting forces. The tangential, radial, and binormal components are calculated as shown:

$$\begin{aligned} dF_t(\Phi,\theta) &= K_{tc}h(\Phi,\theta)db + K_{te}dS \\ dF_r(\Phi,\theta) &= K_{rc}h(\Phi,\theta)db + K_{re}dS \\ dF_a(\Phi,\theta) &= K_{ac}h(\Phi,\theta)db + K_{ae}dS \end{aligned} \quad (22)$$

where dF_t, dF_r, and dF_a (N) are the tangential, radial, and axial components; K_{tc}, K_{rc}, and K_{ac} (N/mm^2) are the shear specific coefficients; K_{te}, K_{re}, and K_{ae} (N/mm) are the edge specific coefficients; dS (mm) is the length of each discrete elements of the cutting edge; h (mm) is the undeformed chip thickness; and db (mm) is the chip width in each cutting edge discrete element. The coordinate transformation relationship is given by Eq.(1). The cutting force model of [30] is not the only one that can be employed in this work. After the undeformed chip thicknesses are obtained, the exponential models [34] or other type of nonlinear models (such as polynomial models) are also can be adopted, only if the cutting force model expression contains the undeformed chip thickness as variable, i.e., $F=F(h)$ in which F is the cutting force and h the undeformed chip thickness.

The summary chart of the proposed model is given in Fig. 8. As it is seen from this chart, the force model consists of four modules, which are calibration, chip thickness, and tool–workpiece engagement region, force validation, and inclination angles optimization modules. The calculation of cutting coefficients is necessary to characterize the couple tool/material and to calculate the cutting force. Different methods of calibrations for cutting force coefficients are discussed. Lee and Altintas [30] used data from orthogonal turning experiments for determining the cutting coefficients with varying chip thickness. Zhu et al. [35] proposed a method of obtaining the cutting force coefficients for ball-end milling using the average chip thickness of slot milling experiments. Oztruk et al. [36] presented an algorithm for calibration of coefficients with inclined slot cutting tests after the contact region determination is analyzed for monotonic free-form surfaces. Cutting force coefficients considering the size effect of undeformed chip thickness and the influence of effective rake angle in ball-end milling are used by Liu et al. [37]. Assuming that the cutting force coefficients of ball-end mill cutting edge varies along the edge and depends on the position angle θ of each element. A similar method referring to [20, 34] for the calculation of the coefficients is adopted in this paper. References [20, 34] discussed the cutting force coefficients considering the influence of cutting edge inclination, which also depends on position angle θ. Linear, quadratic, and cubical polynomial coefficients have been calculated, and it is concluded that the improvement introduced by the quadratic and cubic coefficients is practically inappreciable. However, in this work, to verify the proposed model, it is expected to eliminate the errors from cutting tests as far as possible, so the θ dependent cubic polynomial shear coefficients have been selected, while the plowing coefficients have been considered as constant values. For the Al-7075 aluminum alloy, 18 characterization tests are carried out in Table 5. All characterization tests are half-immersion cutting. The polynomials of the coefficients obtained for the Al-7075 aluminum alloy are performed:

$$\begin{aligned} K_{tc} &= 751.5 + 382\theta + 120.4\theta^2 - 169.6\theta^3 \\ K_{rc} &= 195.4 + 83.1\theta + 35.6\theta^2 + 10.9\theta^3 \\ K_{ac} &= 65.5 - 3.42\theta - 43.7\theta^2 - 72.2\theta^3 \\ K_{te} &= 5.7 \\ K_{re} &= 4.2 \\ K_{ae} &= -1.6 \end{aligned} \quad (23)$$

To demonstrate the model's effectiveness in different cases, comparisons between simulated cutting forces and measured ones are presented. Totally, 34×3 inclination cutting tests were carried out. The cutter runout has been regulated to an acceptable limit through several trials of clamping. All tests are slot cutting at 600 rpm with a constant feed of 120 mm/min and constant cutting depth of 1.5 mm. In order to ensure that only the spherical part of ball-end cutter participates in cutting and keep a constant material removal rate, the lead and tilt angles are restricted, and they are given in Table 6. The inclination angles of the 34 tests are different from each other. As it is easier to define lead and tilt angle in tool path generation software, it should be transformed to angles α and γ before calculation. Two copies of the cutting tests in Table 6 are added to achieve soundness and the measured cutting forces show good accordance between the three groups of tests. The tool paths generated by software Unigraphics, and the machined workpieces are illustrated in Fig. 9.

The comparisons for nine representative cutting conditions of them are shown in Fig. 10. The cutting forces are simulated for *two revolutions* of the milling tool. The full

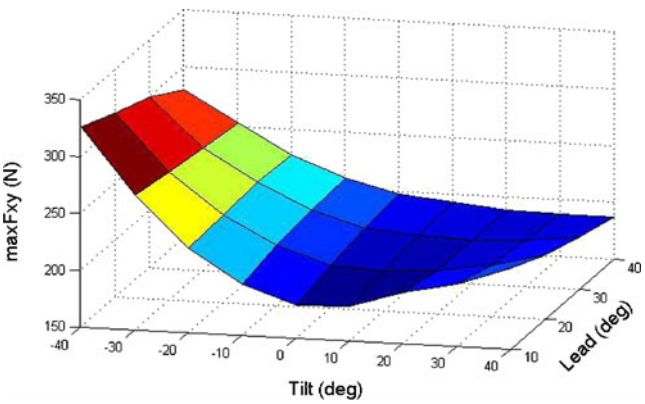

Fig. 11 Maximum forces F_{xy} vs. lead and tilt angles

lines are the simulation results, whereas dotted lines are the measured force values. The forces are plotted in the TCS (*xyz*). The biggest deviations between measured and predicted cutting force occur in several tests with negative tilt angle because of the sticking effect as disc elements start in cutting with zero chip thickness. Sticking effects can be easily observed from the machined surface. The deviation is <10 % in most of the cutting cases.

From Fig. 10, it is seen that inclination angles exert tremendous influence on the values of cutting forces. For example, the maximum value of F_x is over 300 N when lead/tilt angles are 10/−40°, while it is only about 150 N when they are 10/40°. It is because the numbers of disc elements engaged in cutting at a same time varies a lot and contact duration is different with diverse inclination angles, especially tilt angles. This has already been discussed in Section 5 and can be seen intuitionally in Fig. 10.

To optimize the inclination angles. Ozturk and Budak [23] presented a model used as an optimization method while designing five-axis ball-end milling process, and it concludes that the minimum force is obtained when the lead angle is 0° and the tilt angle is 10° for an exact example. However, there is a question that the forces fluctuation is not only due to inclination angles but also the material removal rate. As the cylindrical part of ball-end cutter participates in cutting, material removal rate varies when the tilt angle changes, i.e. greater tilt angle leads to a higher material removal rate. However, the experiments in this work keep a constant material removal rate and assert that the fluctuation of forces is caused only by inclination angles. Another conclusion in [23] is that the effect of the tilt angle on the F_{xy} is more than the effect of the lead angle. However, the internality reason is not given out. In this work a similar graphic is shown in Fig. 11 at a constant material removal rate (the values at (40,40) and (40,−40) is suppositional as it does not meet the requirement that only ball part participates in cut). The minimum F_{xy} is obtained at (10,0) or (40,30). It can be explained: When lead and tilt angle is (10,0), the contact area is near to cutter tip, and value of F_z component is big, which leads to smaller F_{xy}. For the other case at (40,30), the shear coefficients is decreased at higher position angle θ as the polynomials (Eq. 23) have negative cubic terms. This is a compensation that makes the effect of the lead angle on the F_{xy} less than that of the tilt angle.

7 Conclusion

The prediction of cutting force in five-axis ball-end milling is discussed in this paper. The cutting force prediction is based on the decoupled chip thickness calculation model. We give the proposition that the chip thickness of cutting with both lead and tilt angles can be decoupled by the sum of chip thickness distributed from the two individual resolved cutting conditions. The proposition is proved using the intensive numerical analysis and experimental verification. Although the geometrical as well as the kinematics meaning of the proposition is obvious, it cannot be proved easily because of the complex engagement between parts and cutters involved. To assess the accuracy of proposed model, the numerical analysis and experiments are carried out. The material removal volumes based on the proposed chip thickness model are compared with the theoretical results. The cutting experiments validate the cutting force prediction results based on the chip thickness calculation model and the effects of inclination angles on cutting forces are analyzed, which is helpful for the selection of an appropriate tool posture.

Acknowledgments This work was partially supported by the National Basic Research Program of China (2011CB706804), the National Natural Science Foundation of China (51005087), and the National Engineering and Research Center for Commercial Aircraft Manufacturing (SAMC12-JS-15-006). Prof. Xiaoming Zhang acknowledges the support of the Alexander von Humboldt Foundation.

References

1. Erdim H, Lazoglu I, Ozturk B (2006) Feedrate scheduling strategies for free-form surfaces. Int J Mach Tools Manuf 46(7–8):747–757
2. Arizmendi M, Fernández J, Lacalle LNL, Lamikiz A, Gil A, Sánchez JA, Campa FJ, Veiga F (2008) Model development for the prediction of surface topography generated by ball-end mills taking into account the tool parallel axis offset. Experimental validation. CIRP Ann-Manuf Technol 57(1):101–104
3. López de Lacalle LN, Lamikiz A, Sánchez JA, Salgado MA (2007) Toolpath selection based on the minimum deflection cutting forces in the programming of complex surfaces milling. Int J Mach Tools Manuf 47(2):388–400
4. Zhang L (2011) Process modeling and toolpath optimization for five-axis ball-end milling based on tool motion analysis. Int J Adv Manuf Technol 57(9–12):905–916
5. Manav C, Bank HS, Lazoglu I (2011) Intelligent toolpath selection via multi-criteria optimization in complex sculptured surface milling. J Intell Manuf 24(2):349–355
6. López de Lacalle LN, Rodríguez A, Lamikiz A, Celaya A, Alberdi R (2011) Five-axis machining and burnishing of complex parts for the improvement of surface roughness. Mater Manuf Process 26(8):997–1003
7. Kurt M, Bagci E (2011) Feedrate optimisation/scheduling on sculptured surface machining: a comprehensive review, applications and future directions. Int J Adv Manuf Technol 55(9–12):1037–1067
8. Takata S (1993) Generation of a machining scenario and its applications to intelligent machining operations. CIRP Ann Manuf Technol 42(1):531–534
9. Spence A, Altintas Y (1994) A solid modeller based milling process simulation and planning system. Trans ASME J Eng Ind 116(1):61–69
10. El Mounayri H, Spence A, Elbestawi M (1998) Milling process simulation: a generic solid modeller based paradigm. Trans ASME J Manuf Sci Eng 120(2):213–221

11. Imani B, Sadeghi M, Elbestawi M (1998) An improved process simulation system for ball-end milling of sculptured surfaces. Int J Mach Tools Manuf 38(9):1089–1107
12. Kim G, Cho P, Chu C (2000) Cutting force prediction of sculptured surface ball-end milling using Z-map. Int J Mach Tools Manuf 40(2):277–291
13. Fussell B, Jerard R, Hemmett J (2003) Modeling of cutting geometry and forces for 5-axis sculptured surface machining. CAD 35(4):333–346
14. Roth D, Ismail F, Bedi S (2003) Mechanistic modelling of the milling process using an adaptive depth buffer. CAD 35(14):1287–1303
15. Roth D, Gray P, Ismail F, Bedi S (2007) Mechanistic modelling of 5-axis milling using an adaptive and local depth buffer. CAD 39(4):302–312
16. Antoniadis A, Savakis C, Bilalis N, Balouktsis A (2003) Prediction of surface topomorphy and roughness in ball-end milling. Int J Adv Manuf Technol 21:965–971
17. Dongming G, Fei R, Yuwen S (2010) An approach to modeling cutting forces in five-axis ball-end milling of curved geometries based on tool motion analysis. Trans ASME J Manuf Sci Eng 132(4):041004.1–041004.8
18. Lazoglu I, Boz Y, Erdim H (2011) Five-axis milling mechanics for complex free form surfaces. CIRP Ann Manuf Technol 60(1):117–120
19. Gonzalo O, Jauregi H, Uriarte LG, López de Lacalle LN (2008) Prediction of specific force coefficients from a FEM cutting model. Int J Adv Manuf Technol 43(3–4):348–356
20. Lamikiz A, de Lacalle LNL, Sanchez JA, Salgado MA (2004) Cutting force estimation in sculptured surface milling. Int J Mach Tools Manuf 44(14):1511–1526
21. Fontaine M, Moufki A, Devillez A, Dudzinski D (2007) Modelling of cutting forces in ball-end milling with tool–surface inclination. J Mater Process Technol 189(1–3):73–84
22. Ozturk B, Lazoglu I (2006) Machining of free-form surfaces. Part I: analytical chip load. Int J Mach Tools Manuf 46(7):728–735
23. Ozturk E, Budak E (2007) Modeling of 5-axis milling processes. Mach Sci Technol 11(3):287–311
24. Subrahmanyam KVR, San WY, Soon HG, Sheng H (2009) Cutting force prediction for ball nose milling of inclined surface. Int J Adv Manuf Technol 48(1–4):23–32
25. Ferry W, Altintas Y (2008) Virtual five-axis flank milling of jet engine impellers-part I: mechanics of five-axis flank milling. Trans ASME J Manuf Sci Eng 130(1):011005.1–011005.11
26. Tsai C-L, Liao Y-S (2009) Cutting force prediction in ball-end milling with inclined feed by means of geometrical analysis. Int J Adv Manuf Technol 46(5–8):529–541
27. Olvera D, López de Lacalle LN, Urbikain G, Lamikiz A, Rodal P, Zamakona I (2012) Hole making using ball helical milling on titanium alloys. Mach Sci Technol 16(2):173–188
28. Tuysuz O, Altintas Y, Feng H-Y (2013) Prediction of cutting forces in three and five-axis ball-end milling with tool indentation effect. Int J Mach Tools Manuf 66:66–81
29. Ozturk E, Tunc LT, Budak E (2009) Investigation of lead and tilt angle effects in 5-axis ball-end milling processes. Int J Mach Tools Manuf 49(14):1053–1062
30. Lee P, Altintas Y (1996) Prediction of ball-end milling forces from orthogonal cutting data. Int J Mach Tools Manuf 36(9):1059–1072
31. Tunc LT, Budak E (2008) Extraction of 5-axis milling conditions from CAM data for process simulation. Int J Adv Manuf Technol 43(5–6):538–550
32. Cao Q, Xue D, Zhao J, Li Y (2010) A cutting force model considering influence of radius of curvature for sculptured surface machining. Int J Adv Manuf Technol 54(5–8):821–835
33. Wang H, Qin X, Ren C, Wang Q (2011) Prediction of cutting forces in helical milling process. Int J Adv Manuf Technol 58(9–12):849–859
34. Lamikiz A, López de Lacalle LN, Sanchez JA, Bravo U (2005) Calculation of the specific cutting coefficients and geometrical aspects in sculptured surface machining. Mach Sci Technol 9(3):411–436
35. Zhu R, Kapoor SG, DeVor RE (2001) Mechanistic modeling of the ball end milling process for multi-axis machining of free-form surfaces. Trans ASME J Manuf Sci Eng 123(3):369–379
36. Ozturk B, Lazoglu I, Erdim H (2006) Machining of free-form surfaces. Part II: calibration and forces. Int J Mach Tools Manuf 46(7):736–746
37. Liu XW, Cheng K, Longstaff AP, Widiyarto MH, Ford D (2004) Improved dynamic cutting force model in ball-end milling. Part I: theoretical modelling and experimental calibration. Int J Adv Manuf Technol 26(5–6):457–465